Journal of Solid State Chemistry 183 (2010) 1303–1308

Contents lists available at ScienceDirect

Journal of Solid State Chemistry

journal homepage: www.elsevier.com/locate/jssc

Sensitized red luminescence from Ce^{3+}, Mn^{2+}-doped glaserite-type alkaline-earth silicates

Yoshinori Yonesaki *, Takahiro Takei, Nobuhiro Kumada, Nobukazu Kinomura

Interdisciplinary Graduate School of Medical and Engineering, University of Yamanashi, Miyamae 7-32, Kofu 400-8511, Japan

ARTICLE INFO

Article history:
Received 10 February 2010
Received in revised form
31 March 2010
Accepted 5 April 2010
Available online 9 April 2010

Keywords:
Phosphor
Alkaline-earth silicate
Glaserite
Red emission
Energy transfer
Luminescence

ABSTRACT

Bright red luminescence is observed from Ce, Mn-doped glaserite-type alkaline-earth silicates with $M_2BaMgSi_2O_8$ (M: Ba, Sr, Ca) chemical composition. Under UV excitation, Ce-doped $M_2BaMgSi_2O_8$ exhibits strong near-UV emission with asymmetric peak shape. UV-excited Mn-doped $M_2BaMgSi_2O_8$ compounds show visible red emission only when Ce^{3+} ions are doped together. These results indicate that Mn^{2+}-derived red emission is caused by an efficient energy transfer from Ce^{3+} to Mn^{2+}. The red emission becomes intense with an increase in Ba-amount. This trend originates from the relaxation of the selection rule for 3*d*-3*d* transition in Mn^{2+} ions, which is caused by the structural deformation due to Ba^{2+} occupation for layer-pockets.

1. Introduction

Light-emitting devices are desired to fluoresce in various colors with high brightness, as necessary. For instance, a high color rendering index is required for interior lamps and flat panel displays to provide a wider range of expression. Such demands increase the importance of phosphors. Many of the phosphors presently used are obtained by doping radiative transition-metal ions into host material. In particular, Eu^{2+}-activated phosphors have been subjected to considerable number of researches because Eu^{2+} emission, which originates from parity-allowed 5*d*-4*f* electron transition, is intense and covers a wide range of wavelengths, depending on the host lattice. In 1968, Blasse et al. [1] and Barry [2] independently found that $M_3MgSi_2O_8$: Eu^{2+} (M: Ba, Sr, Ca) was suitable for blue-emitting phosphor, and since then, many research groups have devoted their efforts to develop related phosphors. Our group has also investigated their emission properties from the viewpoint of crystal structure [3,4]. Okamoto et al. reported that $(Ba, Sr)_3MgSi_2O_8$: Eu^{2+} efficiently converted the excitation light at 147 nm (resonant line of Xe discharge) and 172 nm (emission band of Xe excimer) to 437-nm emission [5]. Their results assured its applicability to plasma display panels as blue phosphor. Recently, Kim et al. reported that red, green and blue emissions were simultaneously observed from $Ba_3MgSi_2O_8$:Eu^{2+}, Mn^{2+}, which led to a single-phase full-color (RGB) phosphor [6,7]. This finding stimulated researchers engaged in developing phosphors. However, the green light claimed to be from the compound was later assigned to Ba_2SiO_4:Eu^{2+} which appeared as an impurity phase [8]. In a series of the studies on $Ba_3MgSi_2O_8$: Eu^{2+}, Mn^{2+}, it has been clarified that a part of excitation energy was resonantly transferred from Eu^{2+} to Mn^{2+} ions, leading to red emission. Therefore, if appropriately synthesized, $Ba_3MgSi_2O_8$:Eu^{2+}, Mn^{2+} emits in purple because the red emission from Mn^{2+} ions mixes with the residual blue emission from Eu^{2+} ions. Using this codoping effect, Ma et al. have tried to utilize $Ba_3MgSi_2O_8$:Eu^{2+}, Mn^{2+} as a light source for plant cultivation [9]. However, considering the actual process, it is easier to mix red, green and blue phosphors at an arbitral ratio to obtain desired emission color. In this study, we have tried to develop a bright red phosphor using glaserite-type layered alkaline-earth silicate ($M_2BaMgSi_2O_8$, M: Ba, Sr, Ca) as host material. To design such a red phosphor, Ce^{3+} ion was adopted as sensitizer for Mn^{2+} ion in place of Eu^{2+} ion which resulted in the residual blue emission. In Ce^{3+} ion, parity- and spin-allowed electron transition occurs between 4*f*- and 5*d*-orbitals. Since the intense 5*d*-4*f* radiation generally covers ultraviolet (UV) region, Ce^{3+} emission is almost invisible. Therefore, $M_2BaMgSi_2O_8$:Ce^{3+}, Mn^{2+} should appear red under UV excitation if excitation energy is effectively transferred from Ce^{3+} to Mn^{2+}.

2. Experimental section

2.1. Synthesis

All the glaserite-type silicates, $(M_{1.96}Ba_{0.98}Ce_{0.03}Na_{0.03})(Mg_{1-x}Mn_x)Si_2O_8$ (M: Ba, Sr, Ca, x=0–0.30) in molar ratio, were synthesized by solid-state reaction. The charge mismatch for Ce^{3+}

* Corresponding author. Fax: +81 55 254 3035.
E-mail address: yonesaki@yamanashi.ac.jp (Y. Yonesaki).

0022-4596/$ - see front matter © 2010 Elsevier Inc. All rights reserved.
doi:10.1016/j.jssc.2010.04.004

ion at M^{2+}-site was compensated by adding equimolar concentrations of Na^+ ion. The starting materials were $BaCO_3$, $SrCO_3$, $CaCO_3$, magnesium carbonate hydroxide, silica gel, $Ce(OH)_4$, Na_2CO_3 and MnO_2. A small amount of NH_4Cl (about 2 wt%) was used as a flux. Stoichiometric amounts of the raw materials and the flux were mixed and ground by ball milling with zirconia beads in 2-propanol for 4 h. The mixture was heated at 1200 °C for 4 h in a flow of 2%H_2-98%N_2 gas with an intermittent re-grinding. Then, the sample was cooled to near room temperature in the reducing atmosphere.

2.2. Characterization

2.2.1. Identification of crystalline phase

To identify the crystalline phases in each sample, X-ray powder diffraction (XRD) data were collected at room temperature on a Bragg-Brentano diffractometer (RINT-2200 V, Rigaku) operating at 40 kV, 30 mA using Cu$K\alpha$ radiation monochromated with graphite ($\lambda = 1.54058$ Å).

2.2.2. Optical absorption

Room-temperature diffuse reflectance spectra were measured for the prepared samples using an UV-vis spectrometer with an integrating sphere attachment (V-650, JASCO). A diffuse reflectance standard plate (P/N 073G, JASCO PARTS CENTER) was used as a reference. Obtained spectra were converted to optical absorption spectra using a spectrum management program (JASCO).

2.2.3. Photoluminescent properties

Emission and excitation spectra of the prepared samples were measured at room temperature using a spectrofluorometer with a Xe lamp as an excitation source (FP-6500, JASCO).

3. Results and discussion

3.1. Optical absorption of $M_3MgSi_2O_8$-based compounds

Fig. 1 shows the optical absorption spectra of $BaCa_2MgSi_2O_8$-based samples. Since prepared samples were confirmed to be a single phase of glaserite-type crystal by XRD, the difference in spectrum profile originates in dopants. No specific absorption is observed from the host crystal in the measured wavelength range (Fig. 1(a)) while the Ce-doped sample shows broad absorption peaks in the range 200–400 nm (Fig. 1(b)). These five bands correspond to 4*f*-5*d* electron transitions in Ce^{3+} ions. The Mn-doped sample exhibits extremely weak and strong absorption at 423 nm and below 350 nm, respectively. The former originates from $^6A_1 - {}^4A_1$, ^4E (^4G) intra-shell transition in Mn^{2+} ions. The latter may be attributed to charge transfer transition from ligand

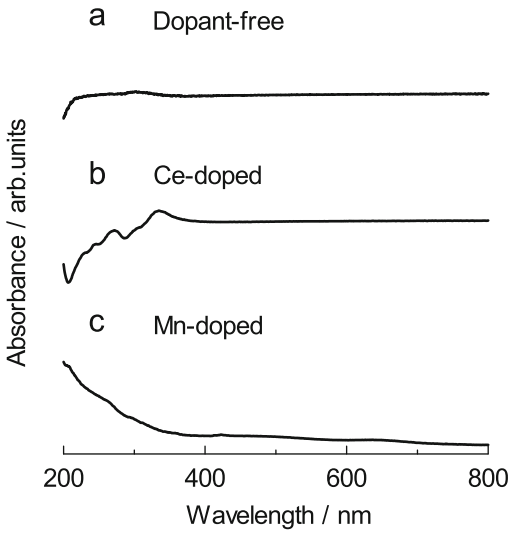

Fig. 1. Optical absorption spectra of $BaCa_2MgSi_2O_8$-based samples; $BaCa_2MgSi_2O_8$ (a), $(Ba_{0.98}Ca_{1.96}Ce_{0.03}Na_{0.03})MgSi_2O_8$ (b) and $BaCa_2(Mg_{0.80}Mn_{0.20})Si_2O_8$ (c).

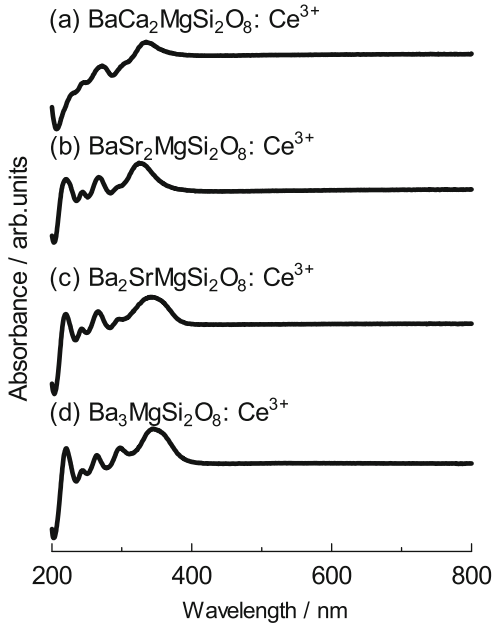

Fig. 2. Optical absorption spectra of Ce-doped $M_2BaMgSi_2O_8$ (*M*: Ba, Sr, Ca) compounds; $(Ba_{0.98}Ca_{1.96}Ce_{0.03}Na_{0.03})MgSi_2O_8$ (a), $(Ba_{0.98}Sr_{1.96}Ce_{0.03}Na_{0.03})MgSi_2O_8$ (b), $(Ba_{1.96}Sr_{0.98}Ce_{0.03}Na_{0.03})MgSi_2O_8$ (c) and $(Ba_{2.94}Ce_{0.03}Na_{0.03})MgSi_2O_8$ (d).

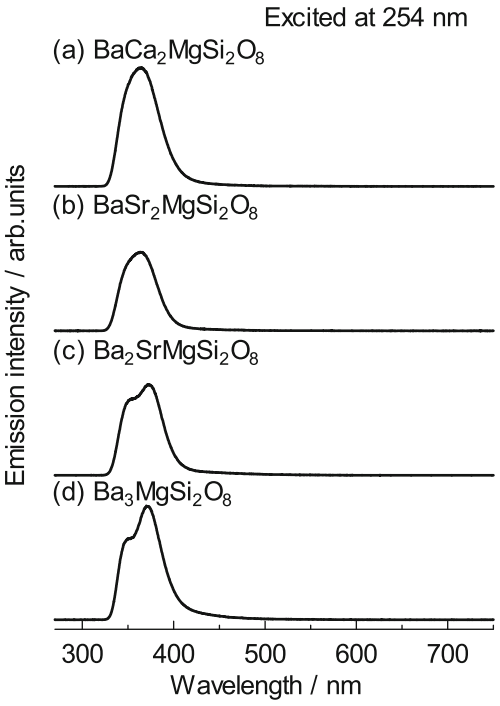

Fig. 3. Emission spectra of Ce-doped $M_2BaMgSi_2O_8$ (*M*: Ba, Sr, Ca) under 254-nm excitation; $(Ba_{0.98}Ca_{1.96}Ce_{0.03}Na_{0.03})MgSi_2O_8$ (a), $(Ba_{0.98}Sr_{1.96}Ce_{0.03}Na_{0.03})MgSi_2O_8$ (b), $(Ba_{1.96}Sr_{0.98}Ce_{0.03}Na_{0.03})MgSi_2O_8$ (c) and $(Ba_{2.94}Ce_{0.03}Na_{0.03})MgSi_2O_8$ (d).

oxide ions to Mn^{2+} ion. Similar results were obtained from the other $M_2BaMgSi_2O_8$-based compounds. Fig. 2 shows the optical absorption spectra for Ce-doped $M_2BaMgSi_2O_8$ samples. The five 5*d*-bands appear at similar wavelengths, which means that Ce^{3+} ions are in similar coordination environments. From the five peak wavelengths, the crystal field splitting ε_{cfs} and the centroid shift ε_c were calculated for the Ce^{3+} 5*d* levels. They were about 16,300 and 13,800 cm^{-1}, respectively. These values agree well with those of simple oxides [10].

3.2. Emission from Ce-doped $M_2BaMgSi_2O_8$

Ce-doped $M_2BaMgSi_2O_8$ (*M*: Ba, Sr, Ca) compounds exhibited near-UV emission under UV excitation due to the appearance of 5*d*-bands (Fig. 2). Fig. 3 shows the emission spectra for the Ce-doped samples under 254-nm excitation. Ce-derived emission covers 350–450 nm range. The peak broadness is characteristic of 5*d*-4*f* electron transition in trivalent Ce ions. Generally, Ce^{3+}-derived emission peak has asymmetric doublet character because of the spin-orbital splitting of the ground state ($^2F_{5/2}$ and $^2F_{7/2}$) with an energy separation of about 2000 cm^{-1}. The near-UV emission peaks seen in Fig. 3 also have asymmetric shape. To interpret the asymmetry, we tried to resolve the emission peak into two Gaussian bands. Least square fitting revealed that the near-UV peaks were composed of the peak at 344–347 nm and that at 360–370 nm. The energy differences between the fitted peaks are listed in Table 1. They are smaller than the value expected from $^2F_{5/2}$ and $^2F_{7/2}$ levels, especially for $BaCa_2MgSi_2O_8$:Ce^{3+}. This result suggests the possibility that the asymmetric emission peak reflects not only the ground state splitting but also multi-site occupation of Ce^{3+} ions. Figs. 4(a)-(d) show the excitation spectra for both tails of the overall near-UV emission band. These excitation peaks correspond to the split *d*-band energy for Ce^{3+} ion under the influence of crystal field. Only $BaCa_2MgSi_2O_8$:Ce^{3+} exhibits slight difference in spectrum shape within 230–280 nm (Fig. 4(a)). The spectrum for shorter wavelength side (329.3 nm) can be regarded as superposition of that for longer wavelength side (420.2 nm) and another weak emission component which shows at least one excitation band at

Table 1.
Energy difference of the two Gaussian peaks fitted to Ce-derived asymmetric emission peak.

Composition of host material	Energy difference (cm^{-1})
$BaCa_2MgSi_2O_8$	1612
$BaSr_2MgSi_2O_8$	1628
$Ba_2SrMgSi_2O_8$	1744
$Ba_3MgSi_2O_8$	1840

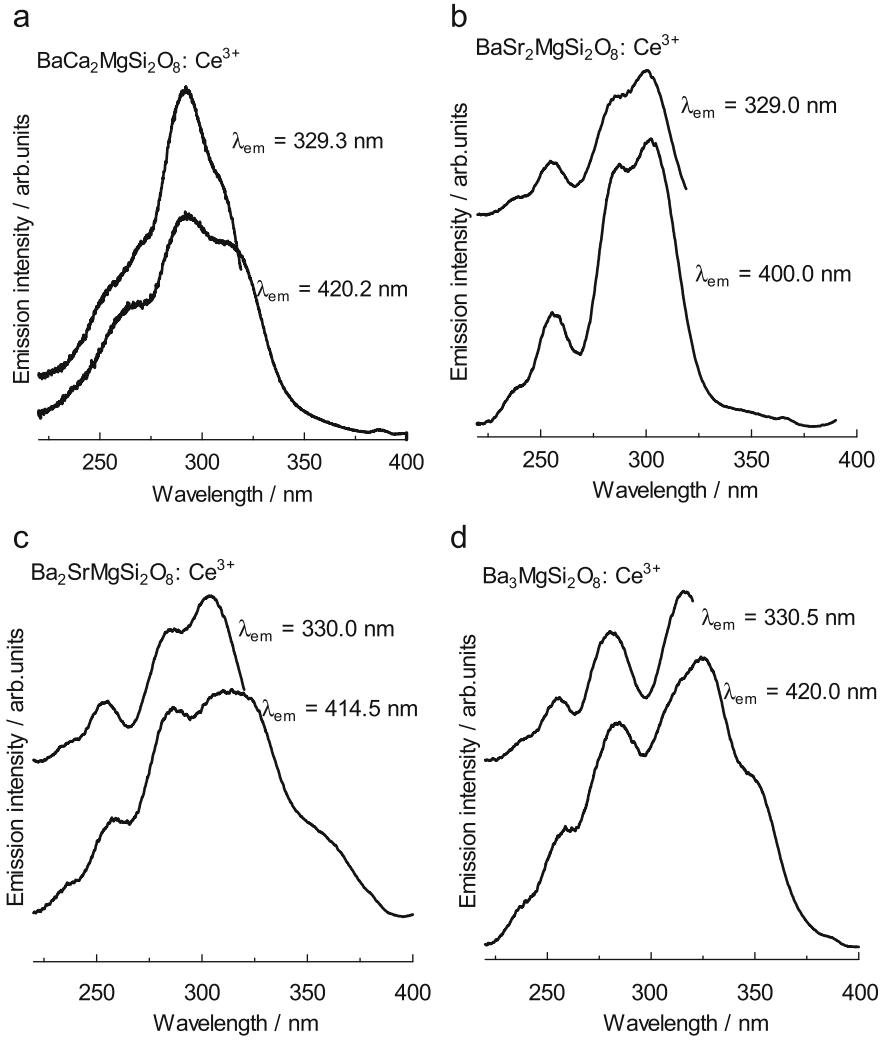

Fig. 4. Excitation spectra for both tails of the whole emission peak; $(Ba_{0.98}Ca_{1.96}Ce_{0.03}Na_{0.03})MgSi_2O_8$ (a), $(Ba_{0.98}Sr_{1.96}Ce_{0.03}Na_{0.03})MgSi_2O_8$ (b), $(Ba_{1.96}Sr_{0.98}Ce_{0.03}Na_{0.03})MgSi_2O_8$ (c) and $(Ba_{2.94}Ce_{0.03}Na_{0.03})MgSi_2O_8$ (d).

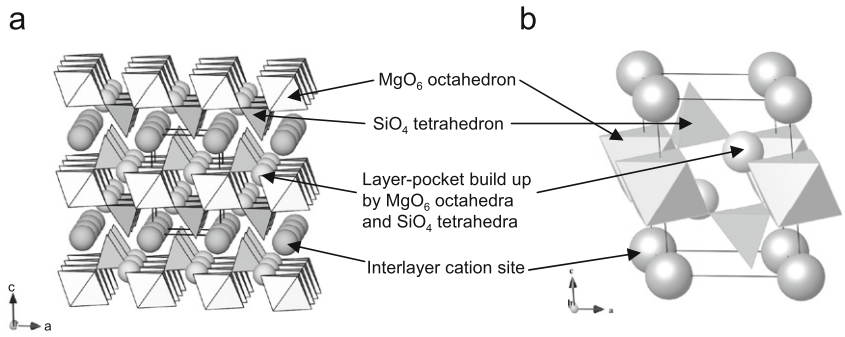

Fig. 5. Glaserite-type crystal structure illustrated with MgO_6 octahedra and SiO_4 tetrahedra. This figure was drawn by VESTA [11].

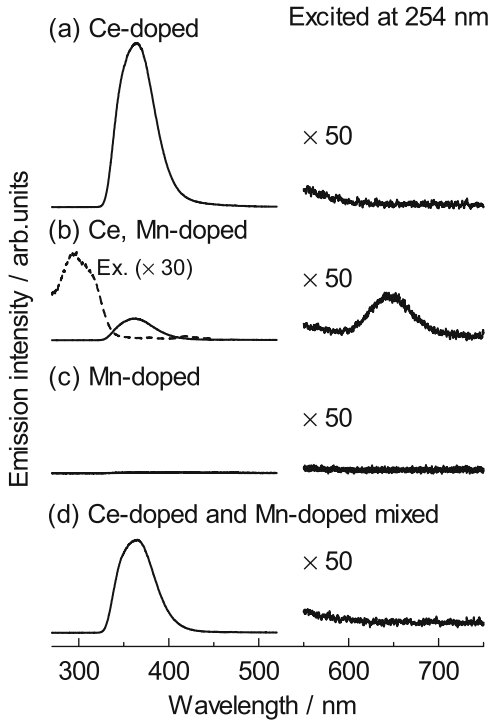

Fig. 6. Emission spectra of Mn-containing $BaCa_2MgSi_2O_8$-based samples under 254-nm excitation; $(Ba_{0.98}Ca_{1.96}Ce_{0.03}Na_{0.03})MgSi_2O_8$ as reference (a), $(Ba_{0.98}Ca_{1.96}Ce_{0.03}Na_{0.03})(Mg_{0.80}Mn_{0.20})Si_2O_8$ (b), $BaCa_2(Mg_{0.80}Mn_{0.20})Si_2O_8$ (c) and mixed sample of a and c in equal amount (d). Dashed line shown in (b) is the excitation spectrum for 645.0 nm (Mn^{2+}-derived) emission for $(Ba_{0.98}Ca_{1.96}Ce_{0.03}Na_{0.03})(Mg_{0.80}Mn_{0.20})Si_2O_8$.

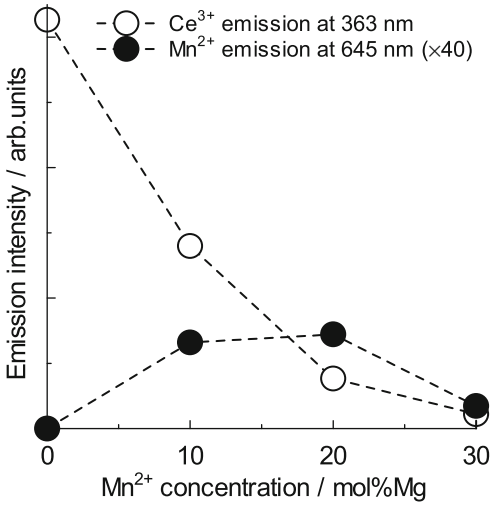

Fig. 7. Mn-concentration dependence of Ce^{3+}- and Mn^{2+}-emission intensities for $(Ba_{0.98}Ca_{1.96}Ce_{0.03}Na_{0.03})(Mg_{1-x}Mn_x)Si_2O_8$ (254-nm excitation).

267 nm. The two different sets of excitation bands indicate the presence of Ce^{3+} ions at distinct crystallographic sites (or under different coordination environments). As reported for Eu^{2+}-doped $BaCa_2MgSi_2O_8$ [3,4], the near-UV emission is ascribed to both Ce^{3+} ions at interlayer site and layer-pocket (Fig. 5). The weakness of the latter emission component may reflect the low Ce^{3+}-occupancy for the corresponding site (the two distinct crystallographic sites are heterogeneously substituted by Ce^{3+} ions).

3.3. Emission properties of Ce, Mn-codoped $BaCa_2MgSi_2O_8$

Ce, Mn-codoped $BaCa_2MgSi_2O_8$ showed red emission under UV excitation. Fig. 6(b) shows the emission spectrum for a Ce, Mn-codoped sample. In this spectrum, a new emission peak can be seen at around 645 nm. This peak originates from $^4T_1(^4G)$-$^6A_1(^6S)$ transition in Mn^{2+} ions at Mg-site. However the 645-nm emission cannot be confirmed from the sample which contains only the same amount of Mn^{2+} ions (Fig. 6(c)). This is because 3*d*-3*d* transition in Mn^{2+} ion is parity- and spin-forbidden. These results indicate that Mn^{2+} ions are effectively excited only in the presence of Ce^{3+} ions. An excitation spectrum monitoring the Mn^{2+}-derived emission (dashed line in Fig. 6(b)) has similar profile with the excitation bands in Fig. 4(a). The similarity implies that a part of energy absorbed by Ce^{3+} ions was transferred to Mn^{2+} ions. In Fig. 7, Ce^{3+}- and Mn^{2+}-emission intensities of Ce, Mn-codoped $BaCa_2MgSi_2O_8$ are plotted against Mn concentration. With Mn increasing, Ce^{3+} emission weakens and Mn^{2+} emission increases although the Mn^{2+} emission is inhibited when over 30 mol% of Mg is replaced with Mn due to concentration quenching and/or high optical absorbance of the sample itself (Fig. 1(c)). The Mn-concentration dependence also supports the energy transfer contribution. It is considered that the energy transfer proceeds by Förster resonance energy transfer (FRET) mechanism (energy transfer via electric multipole-multipole interaction) for the following two reasons; (i) Ce, Mn-codoped sample exhibited no clear excitation band at Ce^{3+}-emission wavelengths (Fig. 6(b)) and (ii) Peak profile of Ce^{3+} emission does not change before and after Mn-addition. To identify the ET process, emission spectrum was measured for the mixture of Ce-doped and Mn-doped samples in equal amount. In this sample, short-range interactions between Ce^{3+} and Mn^{2+} ions could be practically ignored because Ce^{3+} and Mn^{2+} ions were in separate grains. Fig. 6(d) shows the emission spectrum for the mixed sample. While Ce^{3+}-derived peak is clearly seen, Mn^{2+}-derived one is not observable. This result means that Mn^{2+}-emission was achieved

by short-range interactions, such as multipole-multipole interactions, between Ce^{3+} and Mn^{2+} ions. Therefore, a non-radiative energy transfer (FRET) process should be dominant for Mn^{2+}-derived red emission. Probably dipole-quadrupole interaction plays an important role in the FRET process, as suggested for Eu, Mn-doped BAM [12].

3.4. Dependence of Ce^{3+}, Mn^{2+}-derived emission on alkaline-earth metal (M^{2+}) ions

Fig. 8 shows the emission spectra of Ce, Mn-doped $M_2BaMgSi_2O_8$ (M: Ba, Sr, Ca) compounds. As Ba-amount increases, Mn^{2+}-derived emission becomes more intense and shows blue-shift. The former result can be explained from the structural viewpoint. Glaserite-type structure (S.G. $P\bar{3}m1$) is constructed from the layers build up by corner-sharing MgO_6 octahedra and SiO_4 tetrahedra. Considering ionic radius, Mn^{2+} ion (0.970 Å) possibly occupies Mg-site. Between the layers, there are three sites for alkaline-earth metal ions; one is at the center of the interlayer space and the remaining two are at layer pockets surrounded by three MgO_6 octahedra and four SiO_4 tetrahedra (Fig. 5). Because of the large radius, Ba^{2+} ion tends to be excluded from the layer pocket (that is, Ba^{2+} ion preferentially occupies interlayer site). However, when Ba amount exceeds 1/3 of *M* atom ($Ba_2SrMgSi_2O_8$ and $Ba_3MgSi_2O_8$ in the present case), Ba^{2+} ion inevitably sites at the layer pocket [4]. Such misfit occupation distorts surrounding layer-framework and, consequently, lowers Mg-site symmetry as shown in Fig. 9. According to a neutron diffraction analysis, $Ba_3MgSi_2O_8$ has superstructure with lower space-group symmetry $P\bar{3}$ which cannot be specified by X-ray diffraction [13]. We consider that the lowered site symmetry relaxes the selection rule for 3*d*-3*d* transition in Mn^{2+}, which leads to the intense red emission in the Ba-rich samples. Actually, Mn-doped Ba-rich samples exhibited a weak red emission under UV excitation even if Ce was not doped (Fig. 10). Such luminescence cannot be observed so clearly from $BaCa_2MgSi_2O_8$- or $BaSr_2MgSi_2O_8$-based sample. These phenomena assure partially allowed electric dipole transition in Mn^{2+} ions for Ba-rich samples. Dipole-dipole interaction may operate in Ba-rich samples, as well as dipole-quadrupole interaction. On the other hand, the blue-shift accompanied by Ba-amount increase can be explained by the size of coordination polyhedra (MgO_6 octahedra). Blue-shift for Mn^{2+} emission originates from the weakening of the crystal field according to Tanabe-Sugano diagram. Our previous study has revealed that $M_3MgSi_2O_8$ lattice constants α and *c* increase with an increase in average radius of M^{2+} ions [4]. In accordance with the enlargement, six equivalent Mg-O bond lengths increased; Mg-O bond lengths of $BaCa_2MgSi_2O_8$, $BaSr_2MgSi_2O_8$, $Ba_2SrMgSi_2O_8$ and $Ba_3MgSi_2O_8$, calculated from the Rietveld refinement results, were 2.067, 2.102, 2.113 and 2.150 angstrom, respectively. It means that

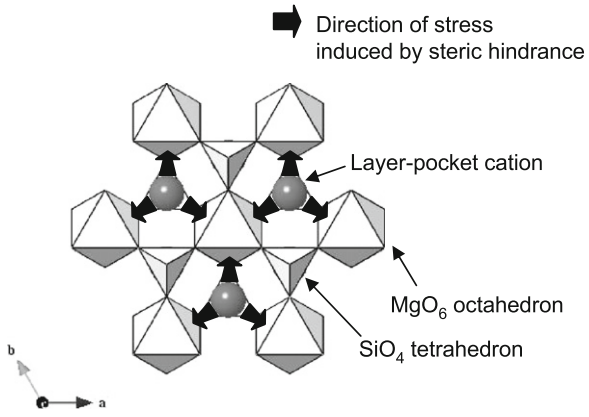

Fig. 9. A schematic illustration of structural stress induced by Ba^{2+} ions at layer-pocket.

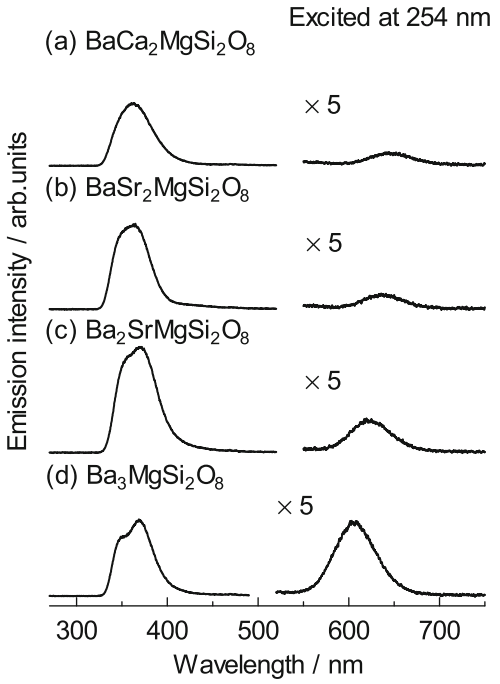

Fig. 8. Emission spectra of Ce, Mn-doped glaserite-type alkali-earth silicates under 254-nm excitation; $(Ba_{0.98}Ca_{1.96}Ce_{0.03}Na_{0.03})(Mg_{0.80}Mn_{0.20})Si_2O_8$ (a), $(Ba_{0.98}Sr_{1.96}Ce_{0.03}Na_{0.03})(Mg_{0.80}Mn_{0.20})Si_2O_8$ (b), $(Ba_{1.96}Sr_{0.98}Ce_{0.03}Na_{0.03})(Mg_{0.80}Mn_{0.20})Si_2O_8$ (c), $(Ba_{2.94}Ce_{0.03}Na_{0.03})(Mg_{0.80}Mn_{0.20})Si_2O_8$ (d).

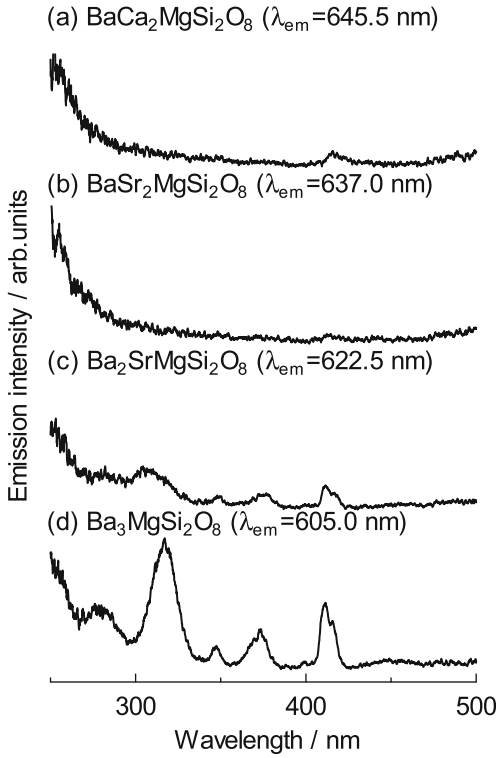

Fig. 10. Excitation spectra of Mn-doped $M_2BaMgSi_2O_8$ (*M*: Ba, Sr, Ca) compounds; $BaCa_2(Mg_{0.80}Mn_{0.20})Si_2O_8$ (a), $BaSr_2(Mg_{0.80}Mn_{0.20})Si_2O_8$ (b), $Ba_2Sr(Mg_{0.80}Mn_{0.20})Si_2O_8$ (c) and $Ba_3(Mg_{0.80}Mn_{0.20})Si_2O_8$ (d).

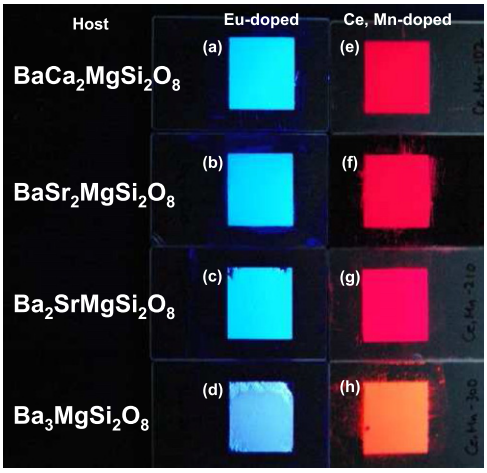

Fig. 11. Emission from glaserite-type alkali-earth silicates under 254-nm light; $(Ba_{0.99}Ca_{1.99}Eu_{0.02})MgSi_2O_8$ (a), $(Ba_{0.99}Sr_{1.99}Eu_{0.02})MgSi_2O_8$ (b), $(Ba_{1.99}Sr_{0.99}Eu_{0.02})MgSi_2O_8$ (c) and $(Ba_{2.98}Eu_{0.02})MgSi_2O_8$ (d), $(Ba_{0.98}Ca_{1.96}Ce_{0.03}Na_{0.03})(Mg_{0.80}Mn_{0.20})Si_2O_8$ (e), $(Ba_{0.98}Sr_{1.96}Ce_{0.03}Na_{0.03})(Mg_{0.80}Mn_{0.20})Si_2O_8$ (f), $(Ba_{1.96}Sr_{0.98}Ce_{0.03}Na_{0.03})(Mg_{0.80}Mn_{0.20})Si_2O_8$ (g), $(Ba_{2.94}Ce_{0.03}Na_{0.03})(Mg_{0.80}Mn_{0.20})Si_2O_8$ (h). Eu-doped samples were prepared based on Ref. [4].

MgO_6 octahedron monotonically enlarges with M^{2+}-size increasing, which results in the weakening of the crystal field strength.

Finally, emission images of the Ce, Mn-doped samples are shown in Fig. 11, together with those of Eu-doped samples. Red emissions from the Ce, Mn-doped samples were bright enough to perceive with the naked eye. $Ba_3MgSi_2O_8$:Ce^{3+}, Mn^{2+} exhibited the brightest emission among the prepared samples. It is found from the figure that Mn^{2+}-derived emission systematically changes color, depending on alkaline-earth metal ions. Such a systematic color shift was not clearly observed for the blue emission from Eu-doped samples.

Since Ce, Mn-doped $M_2BaMgSi_2O_8$ can be excited only with UV irradiation, the silicate phosphor hardly interrupts blue or green emissions from other phosphors. It means that Ce, Mn-doped $M_2BaMgSi_2O_8$ is applicable for white light source composed of UV light emitting diode coated with RGB phosphors.

4. Conclusions

Ce^{3+}-doped glaserite-type alkaline-earth silicate $M_2BaMgSi_2O_8$ (M: Ba, Sr, Ca) exhibits a strong near-UV emission under UV excitation. Mn^{2+} ions doped into $M_2BaMgSi_2O_8$ show bright red emission if Ce^{3+} ions are doped together. In the Mn^{2+} emission, Förster resonance energy transfer from Ce^{3+} to Mn^{2+} plays an important role. Because Ce^{3+}-derived emission is almost invisible to the naked eye, emission from Ce^{3+}, Mn^{2+}-doped $M_2BaMgSi_2O_8$ totally appears red. The structural distortion around Mn^{2+} ions caused by Ba-addition results in an intensity increase.

Acknowledgments

The present work was supported by the Grant-in-Aid for Young Scientists (B) (No. 20750149 for Y.Y.) from the Ministry of Education, Culture, Sports, Science and Technology (MEXT), Japan. Y.Y. is indebted to the financial support by Nippon Sheet Glass Foundation for Materials Science and Engineering.

References

[1] G. Blasse, W.L. Wanmaker, J.W. Vrugt, A. Brill, Philips Res. Rep. 23 (1968) 189–200.
[2] T.L. Barry, J. Electrochem. Soc. 115 (1968) 733–738.
[3] Y. Yonesaki, T. Takei, N. Kumada, N. Kinomura, J. Lumin. 128 (2008) 1507–1514.
[4] Y. Yonesaki, T. Takei, N. Kumada, N. Kinomura, J. Solid State Chem. 182 (2009) 547–554.
[5] S. Okamoto, Y. Nanba, T. Honma, H. Yamamoto, Electrochem. Solid State Lett. 11 (2008) J47–J49.
[6] J.S. Kim, P.E. Jeon, J.C. Choi, H.L. Park, S.I. Mho, G.C. Kim, Appl. Phys. Lett. 84 (2004) 2931–2933.
[7] J.S. Kim, K.T. Lim, Y.S. Jeong, P.E. Jeon, J.C. Choi, H.L. Park, Solid State Commun. 135 (2005) 21–24.
[8] L. Ma, D. Wang, H. Zhang, T. Gu, Z. Yuan, Electrochem. Solid State Lett. 11 (2008) E1–E4.
[9] L. Ma, D. Wang, Z. Mao, Q. Lu, Z. Yuan, Appl. Phys. Lett. 93 (2008) no. 1144101.
[10] P. Dorenbos, J. Lumin. 99 (2002) 283–299.
[11] K. Momma, F. Izumi, J. Appl. Crystallogr. 41 (2008) 653–658.
[12] S. Kamiya, H. Mizuno, Phosphor Handbook, CRC Press, Boca Raton, FL, 1999.
[13] C.H. Park, S.T. Hong, D.A. Keszler, J. Solid State Chem. 182 (2009) 496–501.